

Research Article

Influence of the ground motion directionality on the global ductility of 3D RC structures

Marco Breccolotti^{*,a}, Mattia Pucci^b

Department of Civil and Environmental Engineering, University of Perugia, via G. Duranti, 93, Perugia, Italy

Article Info

Article history:

Received 14 May 2024

Accepted 03 July 2024

Keywords:

Global ductility;
Framed RC buildings;
Seismic action;
Directionality

Abstract

This study examines the influence of ground motion directionality on global ductility μ_s of framed reinforced concrete structures. Suitable values of angle of attack θ , longitudinal reinforcement ratio ρ_l , dimensionless axial stress ν and mechanical ratio of transverse reinforcement ω_{wd} were assumed. Detailed nonlinear modeling was adopted to reproduce the behavior of reinforced concrete elements in the plastic field considering, also, the confinement effect on concrete mechanical properties. Nonlinear static simulations were carried out with the capabilities of the OpenSees code to evaluate the capacity curves and the corresponding global ductility. The results show that plastic hinges develop on the columns for the combined effect of bending moments transmitted by the beams framing into the same joint for values of the angle θ equal to 30° and 45°. Consequently, the formation of soft-storey mechanisms significantly reduces the global ductility μ_s . A design formula is proposed to avoid such collapse mechanism for framed reinforced concrete structures in ductility class high.

© 2024 MIM Research Group. All rights reserved.

1. Introduction

It is known that one of the most relevant actions that can affect reinforced concrete (RC) framed structures is represented by the seismic action. In the last decades, scientific research has made great advances both on the characterization of the seismic action, on the definition of building structural response and on the optimal exploitation of the materials used in the construction. However, the complexity of this problem still leaves unresolved some aspects that could jeopardize buildings structural safety. Among these aspects can be included the effect of seismic action directionality on the global ductility of framed 3D RC structures.

One of the first researches on this topic was conducted by Park and Paulay [1]. The authors observed that seismic loading applied along an axis different from the principal ones of a building will require column strengths considerably greater than that required for the principal directions. Similar comments were raised decades later by Wilson et al. [2]. Their research demonstrated that the way of combining 100% of horizontal action in one direction plus 30% of the seismic action in the perpendicular direction can underestimate the building seismic demand. The authors also showed that a combination according to the square root of the sum of the squares rule of two 100% seismic actions with respect to any user defined orthogonal axes, provides a structural design which has suitable resistance to seismic motions from all directions.

In the last years several investigations have been carried out to analyze the behavior of 3D frame structures subjected to generally oriented seismic action. Magliulo et al. [3]

*Corresponding author: marco.breccolotti@unipg.it

^a orcid.org/0000-0003-1008-9769; ^b orcid.org/0009-0006-3345-1643

DOI: <http://dx.doi.org/10.17515/resm2024.286st0514rs>

Res. Eng. Struct. Mat. Vol. x Iss. x (xxxx) xx-xx

highlighted how the response of a structural system is significantly influenced by the direction of the earthquake comparing the behavior of regular and irregular buildings subjected to bidirectional seismic actions. According to their findings, a critical angle of the seismic action can modify the displacement demand up to 15% and the rotation of the plastic hinges up to 30%.

Two irregular structures, located in Portugal, with 6 floors above ground and 3 underground floors have been studied by Mosleh et al. [4]. The design of the structural elements was carried out considering national and international regulations, including Eurocode 2 [5]. The assessment of the seismic capacity of both structures was carried out by means of non-linear analysis:

- initially pushover simulations were developed for the main directions of each building;
- subsequently integrated through a series of dynamic simulations that included different artificial accelerograms applied to the base of the structures.

The results of the analysis in terms of maximum displacements of the control points were compared with some international guidelines [6, 7]. The study underlined the importance, during the phase of dimensioning and verification of the structural elements, of understanding the effect of biaxial stresses on columns behavior and the influence of axial load variation as a function of the relative position of the element with respect to the system.

Hosseinpour and Abdelnaby [8] carried out a series of analysis on two eight-story framed RC buildings, one regular and the other one irregular in elevation. Seismic sequences were used in irregular buildings along directions corresponding to significantly different global performances due to variations in stiffness, resistance, and ductility. Studies on vertical irregular buildings have been also performed by Shojaei and Behnam [9] who observed that structures with story irregularities sustain more damage than regular structures.

Subsequently, Garcia et al. [10] evaluated the response of three-dimensional steel buildings of different heights under the action of multiple seismic actions. The investigation was conducted through the application of base accelerations with 5 angles of incidence, respectively of 0°, 22.5°, 45°, 67.5° and 90°. The results of their analyses showed that the angle of incidence influences the interstory drift demands also for steel moment-resisting buildings.

Dang et al. [11] carried out experimental investigations to study the behavior of RC columns with controlled failure modes subjected to uniaxial/biaxial loading. Based on tests results, the authors observed that biaxial loading degrades column deformation capacity, and that this reduction can be even more severe for combination of biaxial loading and high axial force. Similar results were also observed by Breccolotti et al. [12].

Recently, Valenzuela-Beltran et al. [13] presented an in-depth analysis of the parameters that influence the seismic response of reinforced concrete buildings, such as: the global ductility level of the buildings, the post-failure stiffness ratio, the structural resistance and the number of stories of the structure. In this regard, the analyses were carried out on three structures of 6, 9 and 12 floors, each of which provided for different levels of ductility capacity (low, medium, and high). The results of their investigation allowed to notice that the magnitude of residual drift demands (RIDDD) was close to 1%, making these buildings prone to suffer large permanent deformations.

The importance of the problem is evidenced by recent publications on the subject such as that of Zhang and Tao [14] who proposed an iterative method to prevent the soft story failure mode and that by Karki, Oinam and Sahoo [15] and Esfandiari, Zangeneh and

Esfandiar [16] who evaluated several strengthening techniques for RC moment resisting frames.

This work aims at further analyze the suitability of current design procedures provided by structural design codes to deal with relevant seismic biaxial loadings on framed 3D structures and ductility capacity of RC columns. Numerical investigations developed through OpenSees software were developed for this purpose. Finally, a simply additional equation to enforce the strong column – weak beam condition also for general biaxial bending in RC columns is proposed. Future studies will be conducted to assess the influence of stiffness and strength degradation resulting from repeated biaxial earthquake loading as already addressed by Abdelnaby and Elnashai [17] for planar frames.

2. Seismic Design of Framed RC Buildings

The effect of seismic force directionality is considered in design codes by specific combination rules. A complete state-of-the-art review on this topic has been published by Wang et al. [18]. For instance, EN 1998 [19] and ASCE-SEI [20] assume that the orthogonal seismic effects can be simulated by means of combination of two orthogonal response spectra, or through a pair of ground movement recordings, where one of these components is taken at its 100% value and the other one is scaled to a 30% value. While this approach provides a conservatory evaluation of the loading intensity, it doesn't consider possible performances changes of the structural system due to a different direction of the resulting loading system. In the next paragraph the main parameters that can be used to describe such performances, namely material, local and global ductility, are briefly recalled.

2.1. Material, local and global ductility

The intrinsic ductility is the property of the material to develop deformations while maintaining a constant or slightly variable level of stress. It is defined, starting from the $\sigma - \varepsilon$ stress-strain diagram obtained through tensile or compression tests, using the following formula:

$$\mu_{\varepsilon} = \frac{\varepsilon_u}{\varepsilon_y} = 1 + \frac{\varepsilon_p}{\varepsilon_y} \quad (1)$$

where ε_y is the deformation at the elastic limit, ε_u the ultimate deformation and ε_p is the strain excursion in the plastic field. With reference to RC structures, an extremely ductile behaviour can be assumed for the reinforcing steel while concrete exhibits a very fragile stress-strain relationship. Nevertheless, the ductility of the concrete can be improved with the introduction of longitudinal and transverse reinforcements in the structural elements. This behavior, known as confinement, can be responsible of an increase in the concrete ultimate strain that can reach values up to 2% [21]. Local ductility is the property of a section to develop localized plastic deformations without a significant reduction in the load bearing capacity. With reference to flexural ductility, it can be determined for a generic section from the moment-curvature diagram using the following formula:

$$\mu_{\theta} = \frac{\theta_u}{\theta_y} = 1 + \frac{\theta_p}{\theta_y} \quad (2)$$

where θ_y is the curvature at the elastic limit, θ_u is the curvature at the ultimate limit and θ_p is the curvature excursion in the plastic field. To calculate the bending ductility, it is necessary to determine the couples $(M_y; \theta_y)$ and $(M_u; \theta_u)$ respectively in the elastic and plastic range. In general, the parameters that influence the flexural ductility of a RC section are:

- concrete compressive strength: as the resistance of the material increases, local ductility increases too;
- concrete confinement: concrete confined by longitudinal and transverse reinforcement is characterized by ultimate strain greater than the value 0.0035, usually assumed by the standards for unconfined concrete, with a corresponding increase in the local ductility of the section;
- reinforcement ratios: an increase in the reinforcement in the compressed zone determines an increase in ductility of the section; conversely, an increase in the reinforcement in the tensile zone reduces the value of ductility;
- tensile strength and yield strength of steel: the use of more resistant steels or steels with higher yield values leads to a reduction in section ductility;
- axial load: as the normal stress acting on the structural element increases, there is a progressive ductility reduction.

This latter aspect is very relevant for determining the actual ductility of the structural elements, especially for the columns which are subjected to high compressive stresses as well as to biaxial bending. The global ductility is the property of the structure as a whole of developing plastic deformations under seismic action without relevant lessening of the load-bearing capacity. In this case the ductility is evaluated observing force-displacement diagrams with the following formula:

$$\mu_s = \frac{s_u}{s_y} = 1 + \frac{s_p}{s_y} \quad (3)$$

where s_y is the displacement at the elastic limit, s_u is the displacement limit and s_p is the displacement excursion in the plastic field of a point assumed as reference for the entire structure (e.g. centre of the top floor of the building). Global ductility is highly influenced by the type of collapse mechanism. In a framed RC structure at ultimate state, two different collapse mechanisms can occur:

- type L mechanism: the formation of plastic hinges occurs at beams ends.
- type H mechanism: the formation of plastic hinges occurs in the columns just below or just above the joints.

With the former mechanism, higher values of the global ductility are generally met. Conversely, the latter mechanism is often responsible for very low global ductility values.

3. Organization of The Study and Method of Investigation

In order to evaluate the influence of bidirectional actions on the global ductility of framed RC structures, two FE models were analyzed with the software OpenSees [22]. Detailed information on the two case studies is provided in the next paragraphs. The dimensions of beams and columns of these structures were assumed based on experience from projects with similar dimensions and loads. This assumption is not relevant for the purposes of the research work. In fact, the results of the following parametric investigations have been analyzed in terms of several dimensionless parameters whose range of use is defined by structural codes. Both models were subjected to nonlinear static analysis (pushover) with different directions of the seismic action. The columns have been assumed perfectly fixed into the foundation even if it is known that soil-foundation-structure interaction can play a relevant role in the seismic performance of buildings [23]. Parametric investigations were carried out assuming different values of the parameters that mostly influence the structural behavior [24]. Finally, global ductility values were extracted from the bi-linearized force-displacement curves.

3.1. One-Story Building

Model T1 represents a typical yet simple precast RC structure frequently found in low-rise commercial buildings in central Italy. It has a square plan of 10.0 m side, a single floor above ground with a height of 8.0 m and hinged connections between beams and columns in both directions. This structure can be considered as representative of low-rise commercial and industrial RC buildings. A perspective view of the structure with its main dimensions is shown in Fig. 1. The columns have a cross section of 600×600 mm while the beams have dimensions of 400×800 mm. The use of concrete C45/55 is foreseen for both structural elements. The roof has an infinitely rigid behavior in its plan. Steel B450C is used for the longitudinal and transverse reinforcements whose arrangement is shown in Fig. 1.

3.2. Two-Story Building

Model T2 represents a typical residential low-rise cast on site RC building frequently found in low-rise residential buildings in central Italy. It has a rectangular plan 5.0×6.0 m, is made up of two floors above ground with a total height of 6.60 m with continuity connections between beams and columns at each level in both directions. A perspective view of the structure is shown in Fig. 1. The columns have a cross-sectional dimension of 400×400 mm while the beams have cross sections of 400×600 mm. Both floors have an infinitely rigid behavior. Concrete class C25/30 is used for beams and columns and B450C steel is used for longitudinal and transverse reinforcements. The arrangement of steel rebars in the columns and in the beams is shown in Fig. 1.

4. Mechanical Properties of Materials

In order to carefully analyze the seismic behavior of the investigated structures, nonlinear behaviors were assumed for concretes and steel. Their mechanical properties are described in the following. Two different concrete materials have been used in the fiber modelling of every cross-section, one for the concrete cover and one for the concrete core. The FE models assume perfect bonding between steel and concrete, thus neglecting the influence of relative slip between the two materials [25] and ignore joint damage and nonlinearity that may also contribute to the deflection of the structure [26].

4.1. Concrete

It is known that concrete stress-strain relationship plays a non-negligible role in the ductility properties of RC elements [27]. For these reasons, the *Concrete02 Linear Tension Softening* material has been chosen from the OpenSees library to describe the concrete behavior. It models uniaxial concrete material objects with tensile strength and linear tension softening with the following stress-strain relationship proposed by Kent and Park [28], subsequently modified by Park et al. [29]:

$$\frac{\sigma_c}{f_{cd}} = \begin{cases} -\left[2\frac{\varepsilon_c}{\varepsilon_{c1}} - \left(\frac{\varepsilon_c}{\varepsilon_{c1}}\right)^2\right] & \text{for } 0 \leq |\varepsilon_c| \leq |\varepsilon_{c1}| \\ -[1 - Z(\varepsilon_c - \varepsilon_{c1})] & \text{for } |\varepsilon_{c1}| < |\varepsilon_c| \leq |\varepsilon_{c,lim}| \end{cases} \quad (4)$$

$$Z = \frac{0.5}{\varepsilon_{50u} - \varepsilon_{c1}} \quad (5)$$

and where σ_c is the concrete stress, f_{cd} is the design concrete compressive strength, ε_c is the concrete strain, ε_{c1} is the concrete strain at peak strength, ε_{50u} is the strain corresponding to half-peak stress and $\varepsilon_{c,lim}$ is the ultimate concrete strain. The constitutive law and the parameters for modelling confined and unconfined concrete are reported, respectively, in Fig. 2 and Table 1.

The effect of confinement in the concrete columns was considered according to the provision of EN 1992 [5]. In detail, the mechanical design properties of the concrete, in terms of stresses and deformations, have been increased to consider the effect of confinement produced by the longitudinal and transverse reinforcements (stirrups or ties). Although it is known that the effect of confinement also produces effects in the ductility of the beams [30], it has been neglected in the present study.

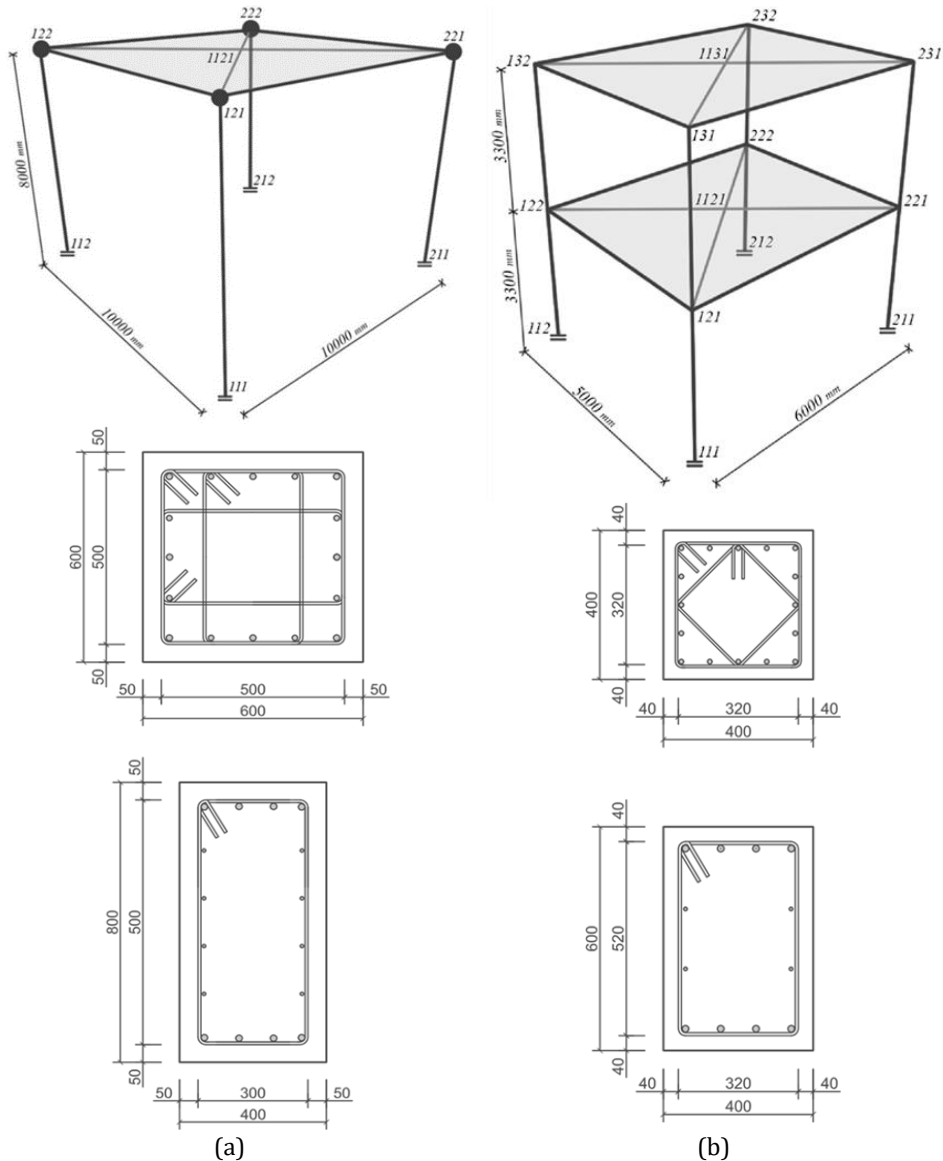


Fig. 1. Perspective view with main dimensions, cross sections and reinforcements of columns and beams (from top to bottom) for (a) model T1 and (b) model T2

In the absence of specific analyses involving the use of analytical models of proven validity, the characteristic strength $f_{ck,c}$ and deformations ($\epsilon_{c2,c}$ and $\epsilon_{cu2,c}$) of the confined concrete can be evaluated according to the following relationships provided by Eurocode 2 [5]:

$$f_{ck,c} = \begin{cases} f_{ck} \cdot \left(1.0 + 5.0 \cdot \frac{\sigma_2}{f_{ck}}\right) & \text{for } \sigma_2 \leq 0.05 f_{ck} \\ f_{ck} \cdot \left(1.125 + 2.5 \cdot \frac{\sigma_2}{f_{ck}}\right) & \text{for } \sigma_2 > 0.05 f_{ck} \end{cases} \quad (6)$$

$$\varepsilon_{c2,c} = \varepsilon_{c2} \cdot \left(\frac{f_{ck,c}}{f_{ck}}\right)^2 \quad (7)$$

$$\varepsilon_{cu2,c} = \varepsilon_{cu} + 0.2 \cdot \frac{\sigma_2}{f_{ck}} \quad (8)$$

where f_{ck} is the concrete compressive strength measured on standard cylinders, σ_2 is the effective lateral confinement pressure; ε_{c2} and ε_{cu} are, respectively, equal to 0.0020 and 0.0035. The effective confinement pressure was determined as $\sigma_2 = \alpha \cdot \sigma_l$ being σ_l the confinement pressure exerted by the transverse reinforcement and α an efficiency coefficient defined as the ratio between the volume $V_{c,eff}$ of effectively confined concrete and the volume V_c of the concrete element. For the rectangular sections of this investigation, the lateral pressure was evaluated, for each main direction, taking into consideration the equilibrium equations in correspondence with the yield stress of the transverse reinforcement, with the following relations:

$$\sigma_{l,x} = \frac{A_{st,x} \cdot f_{yk,st}}{b_y \cdot s} \quad (9)$$

$$\sigma_{l,y} = \frac{A_{st,y} \cdot f_{yk,st}}{b_x \cdot s} \quad (10)$$

where $A_{st,x}$ and $A_{st,y}$ are the areas of the transverse reinforcement in the direction parallel to the main directions X and Y, respectively; b_x and b_y are the dimensions, with reference to the average line of the stirrups, of the confined core in the two corresponding directions; s is the stirrups pitch and $f_{yk,st}$ is the tensile characteristic strength of steel. Once the values of $\sigma_{l,x}$ and $\sigma_{l,y}$ are known, the equivalent lateral pressure can be calculated as $\sigma_l = \sigma_{l,x} \cdot \sigma_{l,y}$. The confinement efficiency coefficient α is a combination of two coefficients, $\alpha = \alpha_n \cdot \alpha_s$, where α_n is a term relating to the arrangement of the transverse reinforcement in the plane of the section and α_s is a term relating to the spacing of the stirrups. For rectangular sections, these two coefficients are equal to:

$$\alpha_n = 1 - \sum_{i=1}^n \frac{b_i}{6 \cdot b_x \cdot b_y} \quad (11)$$

$$\alpha_s = \left[1 - \frac{s}{2 \cdot b_x}\right] \cdot \left[1 - \frac{s}{2 \cdot b_y}\right] \quad (12)$$

being n the total number of longitudinal bars laterally contained by stirrups or ties and b_i the distance between two consecutive contained bars. Finally, the design resistance $f_{cd,c}$ is given by:

$$f_{cd,c} = \frac{\alpha_{cc} \cdot f_{ck,c}}{\gamma_c} \quad (13)$$

where α_{cc} considers the long-term effect on concrete strength and γ_c is the concrete partial safety coefficient.

4.2. Steel

Reinforcement steel has been modeled with the Hysteretic material, also present in the OpenSees library. A strain hardening behavior was modelled by identifying pairs of stress-

strain values as foreseen by EN 1992 [5]. The constitutive law and the parameters used for steel modelling in both case studies are shown, respectively, in Fig. 3 and Table 2.

5. Parametric Investigations

Models T1 and T2 described in chapter 3 were used to perform parametric investigations in which, by varying several geometric and mechanical parameters, 1260 analyses were obtained for each model. To speed up the control and the synthesis of such a great amount of data, the output text files produced by OpenSees were post-processed through an automatic procedure in a MATLAB environment. The following parameters were investigated for both T1 and T2 models:

- angle of application of horizontal forces θ ;
- longitudinal reinforcement ratio ρ_l ;
- dimensionless axial stress ν ;
- mechanical ratio of transverse reinforcement ω_{wd} .

The investigated ranges of these parameters are described in the following paragraphs. The values of these factors used in the parametric analyses are listed in Table 3. Every combination of 4 values of the different parameters has been considered in the analysis for a total number of possible combination equal to $4 \times 7 \times 9 \times 5 = 1260$.

Table 1. Concrete mechanical parameters for models T1 and T2

Model	\$matTag	\$fpc [MPa]	\$epsco	\$fpcu [MPa]	\$epsco	\$lambda	\$ft [MPa]	\$Ets [GPa]
T1	IDConcCover	45.0	0.002	9.0	0.0035	0.1	3.80	70
	IDConcCore	$f_{ck,c}$	$\epsilon_{c2,c}$	$0.2 f_{ck,c}$	$\epsilon_{cu2,c}$	0.1	$0.3 f_{ck,c}^{2/3}$	70
T2	IDConcCover	25.0	0.002	5.0	0.0035	0.1	2.55	70
	IDConcCore	$f_{ck,c}$	$\epsilon_{c2,c}$	$0.2 f_{ck,c}$	$\epsilon_{cu2,c}$	0.1	$0.3 f_{ck,c}^{2/3}$	70

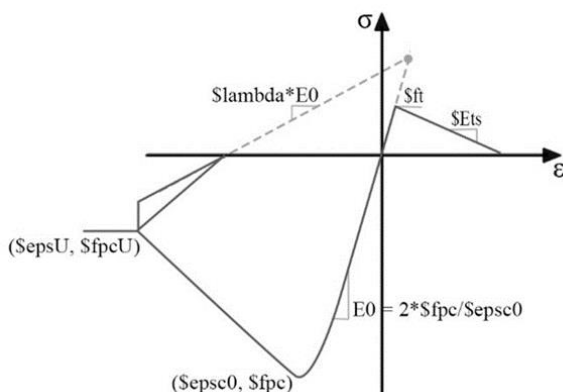


Fig. 2. Hysteretic Stress-Strain Relation for Concrete02 materials

Table 2. Reinforcing steel mechanical parameters

\$matTag	\$e1p	\$sp1 [N/mm ²]	\$e2p	\$s2p [N/mm ²]	\$e3p	\$s3p [N/mm ²]
IDSteel	0.00195	450	0.675	540	0.068	0

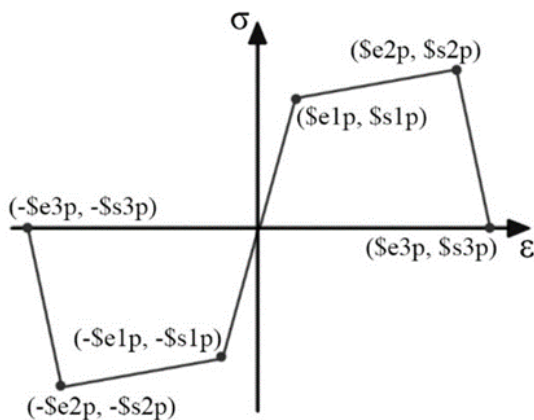


Fig. 3. Hysteretic Stress-Strain Relation for steel rebars

5.1. Angle of Application of Horizontal Forces

Both analyzed models, globally symmetrical with respect to the main axes, have square section columns, with dimensions respectively equal to 600×600 mm and 400×400 mm. The arrangements of the longitudinal reinforcements are also symmetrical with respect to the same main axes. For these reasons, the investigations can be limited to horizontal forces having inclinations θ between 0° and 45°. Intermediate values were chosen every 15°. The lateral force profiles F_i have been determined in proportion to the fundamental mode of vibration. The load values applied along the two directions were obtained based on a decomposition of the force F_i for the i - th floor according to the sine and cosine functions. For instance, with reference to the analysis carried out with an application angle of 15°, the forces along the X direction, $F_{i,x}$ results equal to 0.96 F_i while that along the Y direction, $F_{i,y}$, results equal to 0.25 F_i .

5.2. Longitudinal Reinforcement Ratio

The longitudinal reinforcement ratio is defined as:

$$\rho_l = \frac{\sum A_{si} \cdot n_{bi}}{A_c} \quad (14)$$

where A_{si} is the area of a single rebar, n_{bi} is the number of bars evenly distributed on the cross section and A_c is the total area of concrete. Taking into consideration the provisions of current standards [5], the variability of this parameter was defined in the range $0.01 \leq \rho_l \leq 0.04$ with increments for the intermediate steps of 0.005. The parametric investigations for the longitudinal reinforcement ratio were planned without taking into consideration the commercially available diameters of the reinforcing bars. In each column a total number of rebars n_{bi} equal to 16 was assumed. The rebar diameter and area A_{si} were defined to satisfy the value of the longitudinal reinforcement ratio ρ_l established for the parametric investigation.

5.3. Dimensionless Axial Stress

As well known, the presence of a relevant axial stress is responsible, with the remaining other parameters being unchanged, of a considerable reduction in the local ductility of the elements and, consequently, in the global ductility of the structure. The influence of the axial stress is better investigated referring to the dimensionless axial stress ν , defined by the following relationship:

$$v = \frac{N_{Ed}}{B \cdot H \cdot f_{cd}} \tag{15}$$

where N_{Ed} is the axial force acting on the considered cross-section of the element, B and H are its geometric dimensions and f_{cd} is the concrete compressive design strength. To avoid brittle behaviors, structural standards generally put limits on the maximum values of the dimensionless axial stress v . For instance, the current Italian standard [31] requires that the maximum axial load for RC columns in ductility class “A” (high) and “B” (medium) must not exceed, respectively, 55% and 65% of the maximum compression capacity of the section of concrete only. For these reasons, the range of values $0.10 \leq v \leq 0.50$ have been considered in both models with increments between two consecutive values of 0.05. The value of v equal to $0.10 \div 0.15$ corresponds, approximately, to the dimensionless axial stress acting on the columns of ordinary buildings with geometry like that of the analyzed models. To obtain such values of the dimensionless axial stress, suitable uniformly distributed loads were applied to the beam elements of the floor decks.

5.4. Mechanical Ratio of Transverse Reinforcement

A further parameter that influences the local ductility of structural elements is the mechanical ratio of transverse reinforcement. For the reasons listed in par. 4.1, it is expected an increase in the local ductility of the element as the transverse reinforcement increases, all other conditions being equal. The effect of the transverse reinforcement was fictitiously considered by suitably modifying the constitutive relationship of confined concrete, keeping that of the concrete cover unchanged. The mechanical transverse reinforcement ratio is defined as:

$$\omega_{wd} = \frac{(V_{st,y} + V_{st,z}) \cdot f_{yd}}{V_c \cdot f_{cd}} \tag{16}$$

where $V_{st,y}$ and $V_{st,z}$ are, respectively, the volume of the stirrups along the y and z directions and V_c is the volume of the confined concrete core. According to current standards [19], at the ends of all primary columns, the value of ω_{wd} must be no less than 0.08. Consequently, the values investigated in the parametric analysis were chosen in the range $0.16 \leq \omega_{wd} \leq 0.32$ with intermediate increments equal to 0.04. To consider this parameter in the analysis, for each model and for each value of ω_{wd} , the spacing of the stirrups was properly determined. The values of the parameters α_n and α_s are subsequently calculated to evaluate the confinement coefficient α .

Table 3. Values of the investigated parameters used in the analyses

Parameter	Value								
	1	2	3	4	5	6	7	8	9
Angle Of Application of Horizontal Forces Θ	0°	15°	30°	45°					
Longitudinal Reinforcement Ratio P_L	0.010	0.015	0.020	0.025	0.030	0.035	0.040		
Dimensionless Axial Stress V	0.1	0.15	0.20	0.25	0.30	0.35	0.40	0.45	0.50
Mechanical Ratio of Transverse Reinforcement	0.16	0.20	0.24	0.28	0.32				

Finally, considering the geometric characteristics of the sections, the values of the stresses $\sigma_{l,x}$ and $\sigma_{l,y}$, necessary for the determination of the effective confinement pressure σ_2 , were calculated according to the formulas shown in par. 4.1. The values of the confinement pressures thus obtained are summed up in Tables 4 and 5, respectively for models T1 and T2.

Table 4. Effective confinement pressures for model T1

ω_{wd}	s [mm]	α_n	α_s	α	σ_{lx} [MPa]	σ_{ly} [MPa]	σ_1 [MPa]	σ_2 [MPa]
0.16	155	0.875	0.714	0.624	1.159	1.159	1.159	0.724
0.20	124	0.875	0.767	0.671	1.449	1.449	1.449	0.972
0.24	104	0.875	0.804	0.703	1.739	1.739	1.739	1.223
0.28	89	0.875	0.830	0.727	2.029	2.029	2.029	1.474
0.32	78	0.875	0.851	0.744	2.318	2.318	2.318	1.726

Table 5. Effective confinement pressures for model T2

ω_{wd}	s [mm]	α_n	α_s	α	σ_{lx} [MPa]	σ_{ly} [MPa]	σ_1 [MPa]	σ_2 [MPa]
0.16	108	0.781	0.692	0.540	1.306	1.306	1.306	0.706
0.20	86	0.781	0.749	0.585	1.633	1.633	1.633	0.955
0.24	72	0.781	0.788	0.615	1.960	1.960	1.960	1.206
0.28	62	0.781	0.817	0.638	2.286	2.286	2.286	1.458
0.32	54	0.781	0.839	0.655	2.613	2.613	2.613	1.711

Table 6. Mechanical parameters for confined concrete of model T1

ω_{wd}	σ_2 [MPa]	$f_{ck,c}$ [MPa]	$\epsilon_{c2,c}$	$\epsilon_{cu,c}$	k_1	k_2	k_3
0.16	0.724	48.620	0.002	0.007	1.080	1.167	1.919
0.20	0.972	49.860	0.003	0.008	1.108	1.228	2.235
0.24	1.223	51.110	0.003	0.009	1.136	1.290	2.553
0.28	1.474	52.370	0.003	0.010	1.164	1.354	2.872
0.32	1.726	53.630	0.003	0.011	1.192	1.420	3.192

Table 7. Mechanical parameters for confined concrete of model T2

ω_{wd}	σ_2 [MPa]	$f_{ck,c}$ [MPa]	$\epsilon_{c2,c}$	$\epsilon_{cu,c}$	k_1	k_2	k_3
0.16	0.706	28.530	0.003	0.009	1.141	1.302	2.613
0.20	0.955	29.770	0.003	0.011	1.191	1.418	3.182
0.24	1.206	31.030	0.003	0.013	1.241	1.540	3.756
0.28	1.458	32.290	0.003	0.015	1.292	1.668	4.333
0.32	1.711	33.550	0.004	0.017	1.342	1.801	4.911

At this point, once the effective confinement pressures σ_2 are known, it is possible to calculate the parameters necessary for the mechanical characterization of the confined concrete. However, the determination of the characteristic strengths $f_{ck,c}$ and of the strains $\epsilon_{c2,c}$ and $\epsilon_{cu,c}$ of the confined concrete is not sufficient for the purposes of the parametric analysis. In order to simplify the procedure, the following coefficients, $k_1 = f_{ck,c}/f_{ck}$, $k_2 = \epsilon_{c2,c}/\epsilon_{c2}$ and $k_3 = \epsilon_{cu,c}/\epsilon_{cu}$ have been used in the analysis with f_{ck} respectively equal to 45 MPa and 25 MPa for T1 and T2 models. Tables 6 and 7 show the values obtained for these parameters as the mechanical transverse reinforcement ratio ω_{wd} varies.

6. FE Analyses

As already mentioned, the structural behavior of the two models was analyzed for each different combination of the investigated parameters with the capabilities of the OpenSees software. In order to reduce the approximation errors, especially those related with the definition of the length and behavior of the plastic hinges, diffused plasticity models were implemented through the nonlinear beam column elements.

After having defined the formulations characterizing beams and columns, the cross-sections were discretized into a finite number of fibers for each control point. The fibers model allowed to accurately describe the behavior of structural elements under different load conditions through the determination of the stress-strain states on each single fiber. Therefore, if the number of fibers with which the cross-section is discretized is sufficiently large, the distribution of mechanical non-linearities can be accurately modelled even in a markedly inelastic field.

6.1. Modelling Details

The main assumptions made in the analysis were as follows:

- the control points for the pushover analysis were located at the center of gravity of the last rigid floor;
- a Corotational transformation was adopted for the beams (i.e. an exact geometric transformation of the element stiffnesses from the local to the global system) to follow the excursion in the plastic field of the elements during the execution of the nonlinear analysis;
- P-Delta effects were considered for column elements being the building subjected to relevant lateral displacements;
- the normalized eigenvector values calculated by modal analysis were used to define the shape of lateral force profile to be applied to the models.

6.2. Results of Pushover Simulations

The main results of each analysis can be synthesized with a capacity curve (i.e. a force-displacement curve). In fact, it provides the necessary information for the subsequent determination of global ductility μ_s . Each analysis provided reactions and displacements of the control point in the two main directions X and Y. To allow the comparison of results, base shears V_i and displacements s_i were calculated for each analysis by means of vectors summation. Once the base shear and the displacement for each step or i -th increment are known, the curve of real capacity V-s can be obtained.

6.3. Bilinearization of Capacity Curves

For real systems, the capacity curves generally show similar trends characterized by a first straight branch, corresponding to the linear behavior of the structure, followed by a non-linear path corresponding to the plastic response. To synthesize and compare the seismic behavior of different structures, the curves obtained through nonlinear static analysis must be simplified through linearization. This procedure is briefly recalled in the following.

In literature there are several criteria for linearizing the capacity curves, but different criteria can also provide significantly different results starting from the same input values. The approximation of the curve is the more accurate the smaller the distance, point by point, between the linearized curve and the original one.

Below, reference will be made to the following characteristic points:

- point corresponding to the first yielding of any reinforcement within the structural system with coordinates (x_{sy}, y_{sy}) ;

- point at which the maximum base shear is reached, with coordinates (x_{max}, y_{max}) ;
- point at which the collapse conditions are conventionally assumed to occur, with coordinates (x_{su}, y_{su}) .

The main procedures for identifying the displacement at the elastic limit in a linearized capacity curve have been summarized by Park and include:

- the exact identification of the point corresponding to the first yielding of any reinforcement within the structural system;
- the intersection between the straight-line tangent to the curve in the origin and the tangent line to the capacity curve at its maximum value;
- the intersection between the straight-line passing through the origin of the system and the point of the curve corresponding to a value of 75% of the maximum base shear and the straight-line tangent to the capacity curve at its maximum value;
- the definition of a bi-linear curve obtained through the equality of the subtended area with that of the capacity curve of the structure.

Among these different possibilities, a mixed strategy between methods c and d was chosen in this investigation. In detail, the stiffness of the initial elastic branch was calculated according to method c). It was, thus, imposed the passage of this line through the point $(s_y, V_y = 0.75 \cdot V_{max})$. The ultimate displacement, of coordinates (s_u, V_u) , is identified assuming $V_u = 0.85 \cdot V_{max}$.

The perfectly plastic branch was determined according to method d). Thus, the value of the yielding plateau was determined imposing the equivalence between the area subtended by the bilinear curve up to the displacement value s_u and the area subtended by the real pushover curve up to the collapse point (s_u, V_u) . It can be demonstrated that, imposing this area equivalence, the yielding plateau $V_{y,bil}$ of the bilinear curve results equal to:

$$V_{y,bil} = \frac{V_y}{s_y} \left(s_u - \sqrt{s_u^2 - 2 \frac{s_y}{V_y} A_{push}} \right) \quad (17)$$

Correspondingly, the yielding displacement $s_{y,bil}$ in the bilinear curve is:

$$s_{y,bil} = s_y \frac{V_{y,bil}}{V_y} \quad (18)$$

Finally, the global ductility of the structure μ_s was calculated accordingly to Eq. (3).

7. Results of Parametric Investigations

The 1260 global ductility values obtained for models T1 and T2 are shown in Figs. 4 and 5, respectively. In these figures the ductility values are reported on the vertical axis. In the other two axes are reported the angle of attack of the seismic action θ and the longitudinal reinforcement ratio ρ_l . Different colors are used to distinguish between different values of dimensionless axial stress v . Different shades of the same color represent different values of the mechanical ratio of transverse reinforcement ω_{wd} . From these figures is it clearly observable the negative influence that an angle of attack different from 0° has on the values of the global ductility μ_s .

But it is, indeed, very difficult the observation in these figures of trends and features different from the principal ones. Further observations can be made in different graphs. For instance, in Fig. 6 are shown the results of models T1 and T2 obtained for a constant value of the transverse reinforcement mechanical ratio ω_{wd} equal to 0.28. Each image is relative to a different value of the longitudinal reinforcement ratio ρ_l (from 0.010 at the top to 0.040 at the bottom). The reading and interpretation of the results is facilitated by

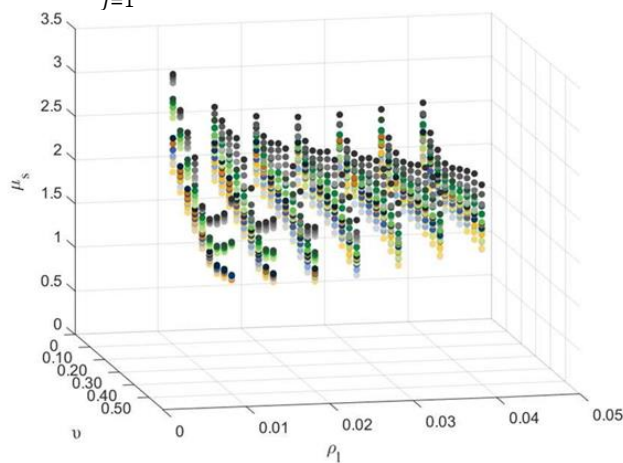
the introduction of trend lines, relative to the same value of the dimensionless axial stress v (from 0.10 depicted with light green to 0.50 represented with dark blu) that connect ductility values obtained for different values of the angle of attack of the seismic action θ (from 0° to 45°).

7.1. Comments on The Obtained Results

The results obtained in terms of global ductility μ_s for model T1 are like those found for the local ductility in another publication [12]. This can be ascribed to the presence of a single global collapse mechanism corresponding to that already identified at the section level. In fact, whatever the direction of the seismic actions, the plasticization in the structural elements is concentrated at the base sections of the columns. Therefore, the angle of application of the seismic action does not determine a variation of the collapse mechanism but at most a reduction of the global ductility values, the latter being function of strength and ductility capacities of the individual columns. Conversely, the parametric analyses carried out for model T2 allow to highlight how the application of bidirectional actions on more complex structures can determine different global behaviors. In fact, the analysis conducted on the two-story model reveal that the development of plastic deformations in the structure is influenced not only by the geometric and mechanical characteristics of the structural elements but also by the angle of application of the horizontal forces.

For low values of the ratio ρ_l (0.01 and 0.015), model T2 behaves according to the soft-story mechanism (type "H") with low global ductility values, regardless of the angle of application of the horizontal force profiles. This result was expected since in these conditions a configuration with strong beam - weak column is obtained, contradicting the basic condition of "Capacity Design":

$$\sum_{i=1}^{n_c} M_{c,Rd,i} \geq \gamma_{Rd} \cdot \sum_{j=1}^{n_b} M_{b,Rd,j} \tag{19}$$



ω_{wd}	Angle 0°	● 0.16	● 0.20	● 0.24	● 0.28	● 0.32
	Angle 15°	● 0.16	● 0.20	● 0.24	● 0.28	● 0.32
	Angle 30°	● 0.16	● 0.20	● 0.24	● 0.28	● 0.32
	Angle 45°	● 0.16	● 0.20	● 0.24	● 0.28	● 0.32

Fig. 4. Complete plot of displacement ductility factors for model T1

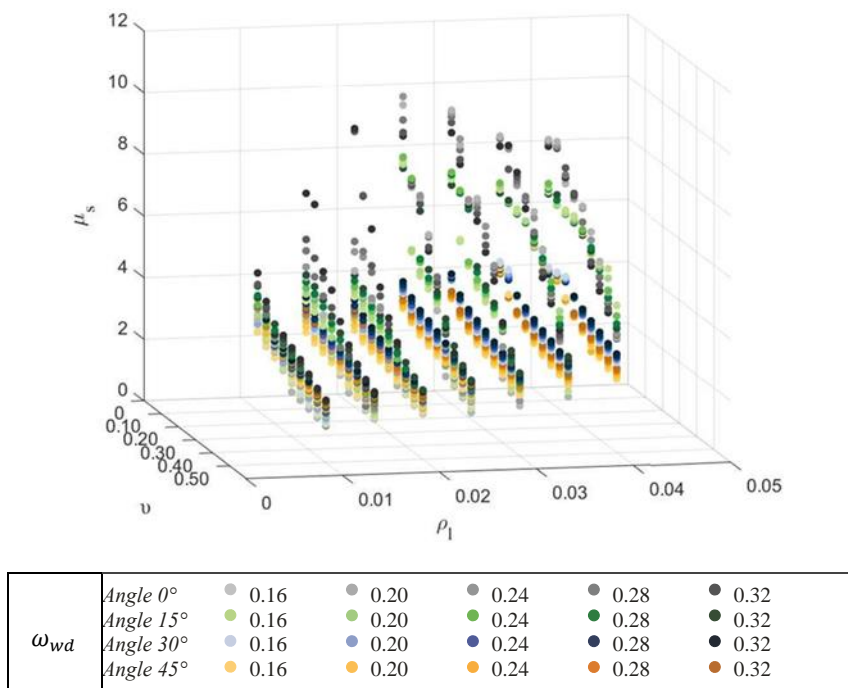


Fig. 5. Complete plot of displacement ductility factors for model T2

where γ_{Rd} is the model uncertainty factor for the design value of resistances, also known as overstrength factor, $M_{c,Rd,i}$ is the bending capacity of the column and $M_{b,Rd,j}$ is the bending capacity of the beams framing into the joint. As the longitudinal reinforcement in the columns increases with unchanged other conditions (mechanical ratio of transverse reinforcement and dimensionless axial stress), an increase in the resisting capacities is obtained. Nevertheless, the transition from the strong beam - weak column mechanism to the strong column - weak beam configuration can be observed only for small values ($\theta = 0^\circ$ and 15°) of the angle of attack. To better understand the physical reasons that determine a decrease in displacement ductility, the progression of the plastic hinges during the analysis was observed. For ease of simplicity, only the configuration of the model at the moment of reaching the displacement corresponding to s_u is considered.

The parametric survey highlights how some angles of application of lateral forces can facilitate the activation of collapse mechanisms other than those commonly expected during the design phase, with consequent effects on the displacement ductility values. The capacity curves shown in Fig. 7, as examples of effective and linearized capacity curves, were obtained by varying the angle of application of the lateral forces θ and the longitudinal reinforcement ratio ρ_l , while the mechanical ratio of the transverse reinforcement ω_{wd} and the dimensionless axial stress ν were kept constant. In the upper part of the figure are shown four images, each one for a different angle of attack θ . In a single image, 7 couples of curves are shown for different values of the longitudinal reinforcement ratio ρ_l . The results obtained by varying the angle θ highlight a decrease in ductility values when the lateral forces are not parallel to one of the main axes of the structural system. In fact, the range of values obtained in the case of $\theta = 0^\circ$ is between 4.00 and 9.15, depending on the longitudinal reinforcement ratio ρ_l . This range of values is maintained unchanged, albeit with some reductions not exceeding 10%, for an application angle of 15° .

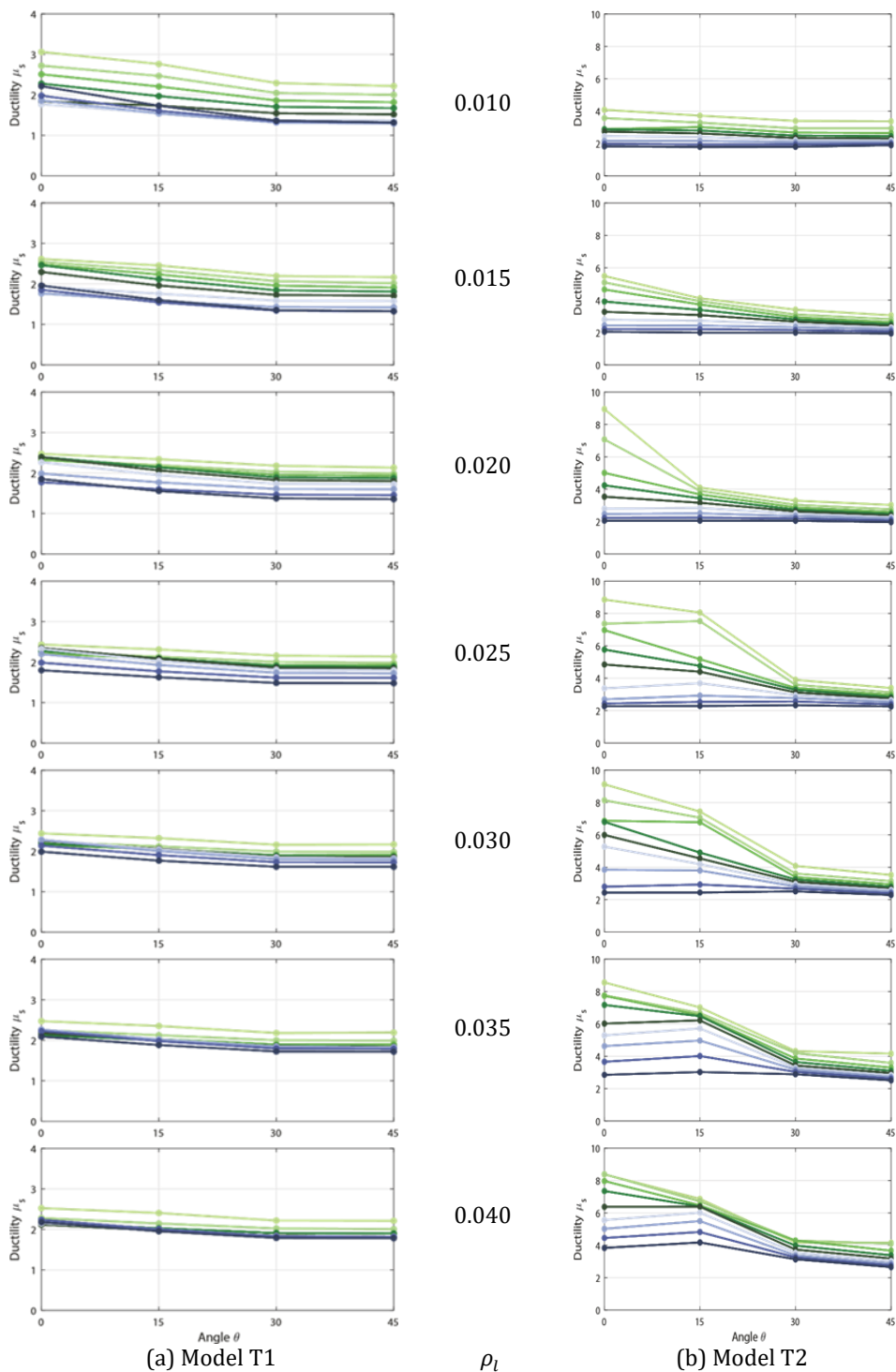


Fig. 6. Ductility values μ_s obtained for $\omega_{wd}=0.28$ and different values of ρ_l (from 0.010 at the top to 0.040 at the bottom) and v (from 0.10 depicted with light green to 0.50 represented with dark blue) for model T1 (a) and model T2 (b)

Conversely, the capacity curves obtained for the remaining angles show global ductility values never higher than 4.50, with ultimate displacements reached by the control point of less than 200 mm. Similarly, the influence of the angle of attack of the seismic forces on the ductility can be highlighted, in the same figure, considering the development of plastic hinges on the structural elements when the displacement s_u is reached. In the lower part of the figure, in fact, are shown 24 images of model T2, one for each combination of the 4 θ and 7 ρ_l values of the previous mentioned capacity curves. In each image:

- the formation of the plastic hinges in correspondence with the elements is highlighted in green for the beams and red for the columns;
- the type "L" collapse mechanism is indicated with a light grey background and the type "H" one with a dark grey background.

Consistently with the capacity curves, the reduction of ductility values as the angle θ increases is conditioned by the mechanism developed during the excursion in the plastic phase. In fact, for angles between 30° and 45° the dominant collapse mechanism is the "H" type, with plasticization in the columns of the first floor and low values of μ_s . The occurrence of this mechanism can be identified in the images shown in the lower part of Fig. 7 characterized by a dark gray background. In these images it is possible to notice the presence of two plastic hinges (red circles) at the ends of all the columns of the first floor, a configuration which corresponds precisely to the "H" type mechanism. This can happen despite the following combinations of seismic actions required from the structural codes, also for non-linear static analysis:

$$E = \begin{cases} E_{Edx} + 0.3E_{Edy} \\ 0.3E_{Edx} + E_{Edy} \end{cases} \quad (20)$$

where E_{Edx} represents the action effects due to the application of the seismic action along the chosen horizontal axis X of the structure and E_{Edy} represents the action effects due to the application of the same seismic action along the orthogonal horizontal axis Y of the structure. While providing for the simultaneous presence of seismic actions on two orthogonal directions, these combinations could not be sufficient to cover all cases to which constructions could be subjected during an earthquake. In fact, the combination rule of Eq. (20) allows to consider only seismic action with inclination in the range $\pm 15^\circ$ respect the mail directions. Although these combinations introduce a seismic intensity slightly higher (104.4%) than the effective one (100%), it is not sure that it reproduces the most demanding condition for the system: any floor mechanisms that are activated by different directions of application of the seismic action are ignored by regulatory provisions. Recalling the content of par. 5.1, since the relationship $F_{i,x} > F_{i,y}$ remains such for the entire analysis, the first yielding will occur in correspondence of beams positioned along the X direction, while the beams located in the Y direction will remain in the elastic range without undergoing yielding.

The final positions of the structural model evaluated at the end of each analysis (achievement of the displacement s_u) are shown in the left image of Fig. 8. In the same figure, in its right part, are shown the trajectories of the control point of the system with their corresponding X and Y displacements. For the reasons described above, if plasticization occurs in the beams, the structure tends to deform almost completely along the direction for which a reduction in stiffness is obtained. This effect is particularly evident for analysis carried out with application angles between 15° and 30°: the dominant displacements along X direction confirm how the structure has developed a post-elastic mechanism with plasticization at the end sections of the beams. In some cases, it is also evident a sudden increase of the displacement in the Y direction. This occurs when plastic hinges appear in the columns.

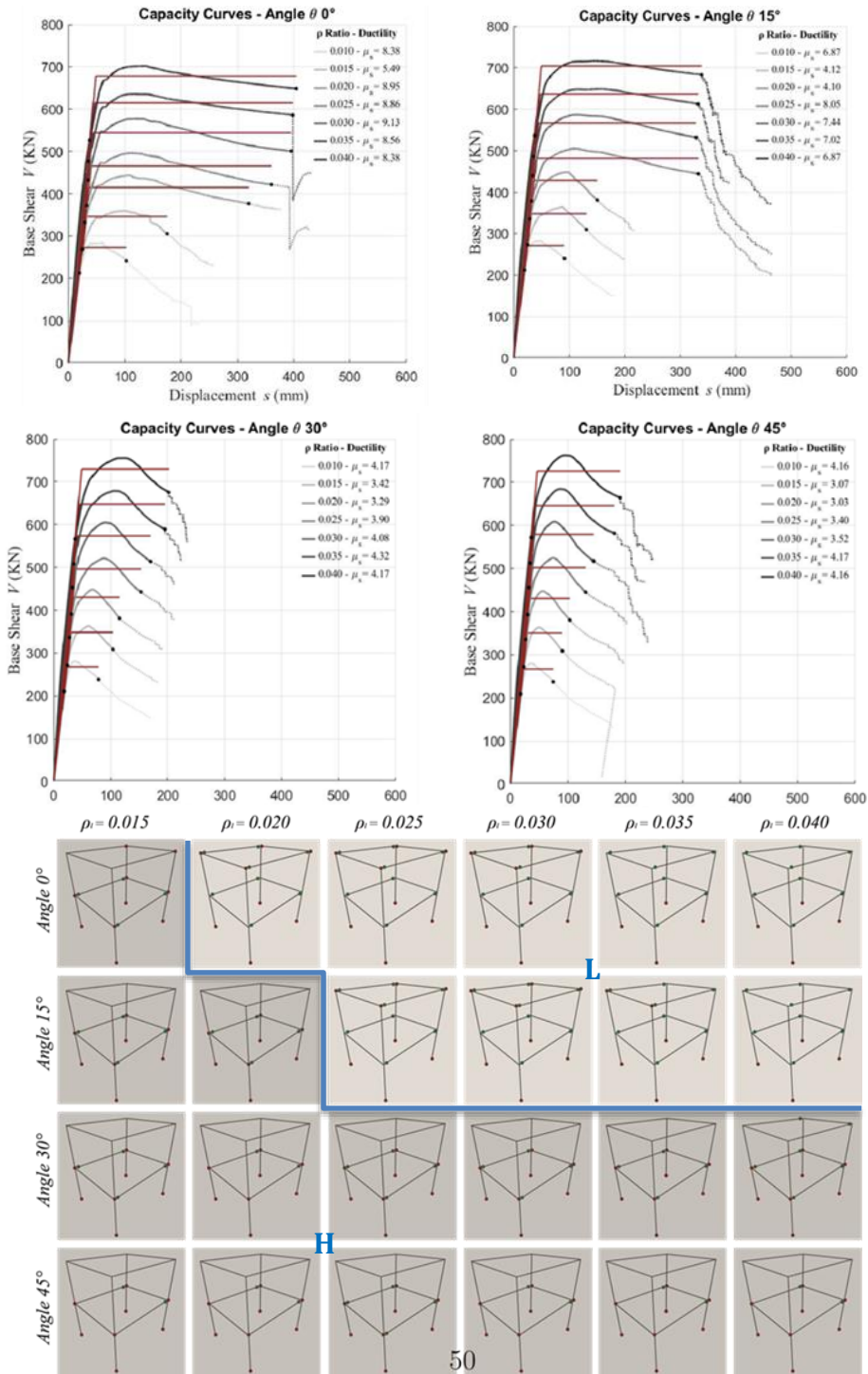


Fig. 7. Failure mechanisms in model T2 for different values of longitudinal reinforcement ratio and angles of attack. Red and green dots: plastic hinges in columns and beams, respectively. Dark and light grey background: “H” and “L” mechanism, respectively

7.2. Main Outcomes and Proposal for Behavior Improvements

The main outcomes of this investigation can be resumed as follows:

- for high values of the angle of attack (θ equal to 30° and 45°) a relevant reduction of the global ductility μ_s can be observed;
- for high values of the angle of attack (θ equal to 30° and 45°) collapses occur according to a soft-story mechanism. The rule relating to the hierarchy of bending resistances applied separately at the node in the two main directions may no longer be sufficient when dealing with seismic actions having direction very different from the principal directions of the system.

The first observation derives by the reduction of flexural strength for biaxially loaded rectangular or square columns when the vector moment is inclined respect the principal axis of the section [32]. An improvement to this behavior can be achieved by simply moving some of the rebars placed along the sides of the column section towards the vertexes of the section itself. This is shown, for instance, in Fig. 9 (left) for the column of model T2. This modified distribution, without reducing the concrete confinement and the flexural resistance towards the bending moments along the principal axes, allows obtaining greater resistance and ductility against biaxial bending loadings. The positive effect of this expedient in the distribution of the reinforcing bars can be noted in the comparison between the capacity curves show in Fig. 10. For a standard rebars distribution the maximum ductility value μ_s is equal to 3.75. It raises up to 4.25 (+13.3 %) for the modified distribution without affecting the behavior of the section for axially loaded column in one direction only and without cost increase.

Nevertheless, this simple trick is not always sufficient for a relevant improvement of the seismic behavior. Such drawback can be ascribed to the inadequacy of the control laws of Eq. (19) for both principal directions to guarantee the capacity design for seismic actions having directions different from the principal axis of the section. In these cases, especially for structures designed assuming a ductility class high (DCH) according to EN 1998 [19], it would be recommended also checking the following condition:

$$\sum_{i=1}^{n_c} M_{c,Rd,i,45^\circ} \geq \gamma_{Rd} \cdot \sqrt{\left(\sum_{i=1}^{n_{cx}} M_{b,Rd,i,x} \right)^2 + \left(\sum_{j=1}^{n_{cy}} M_{b,Rd,j,y} \right)^2} \quad (20)$$

where $M_{c,Rd,i,45^\circ}$ is the minimum resisting bending moment of the column along a direction inclined of $\pm 45^\circ$ respect one of the principal directions, $M_{b,Rd,i,x}$ and $M_{b,Rd,j,y}$ are the bending strengths of beams in the x and y principal directions, respectively.

This condition requires that the resisting moment of the columns should be greater than the vector combination of the resisting moments of the beams converging in the joint. The effects of this provision have been checked on model T2 where the dimensions of the columns have been increased to 500×500 mm (Fig. 9, right) in order to satisfy Eq. (20) without varying the longitudinal reinforcement ratio ρ_l values. The results show that the ductility increase is evident starting from values of ρ_l equal to 0.02 for which a ductility value of 5.93 is achieved (Fig. 11). This value corresponds to an increase of +58.1% compared to the maximum ductility value obtained in the case of the 400×400 mm column with standard reinforcement pattern.

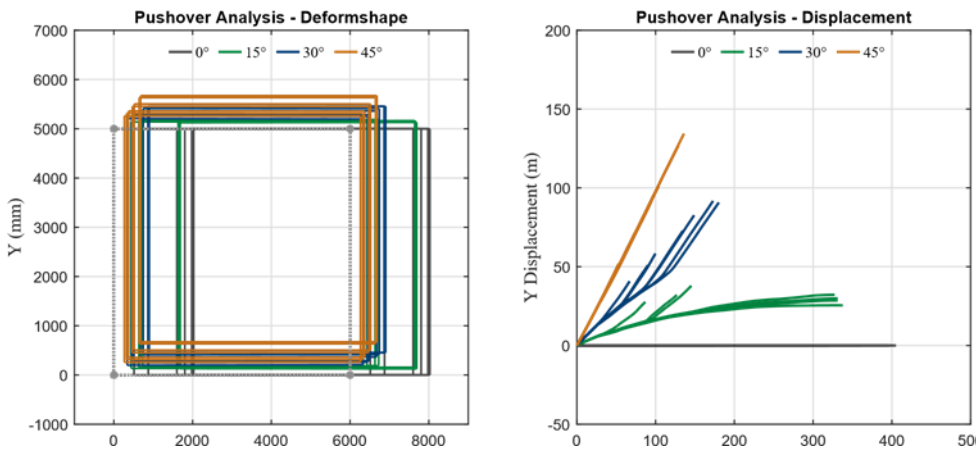


Fig. 8. Planar positions (left) and displacements of the control point (right) at the end of pushover analysis for model T2

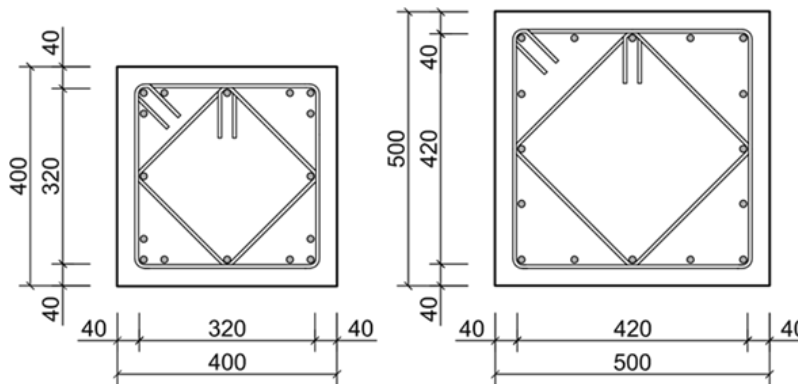


Fig. 9. Section 400×400 mm with improved steel rebars distribution (left) and section 500×500 mm satisfying Eq. (21)

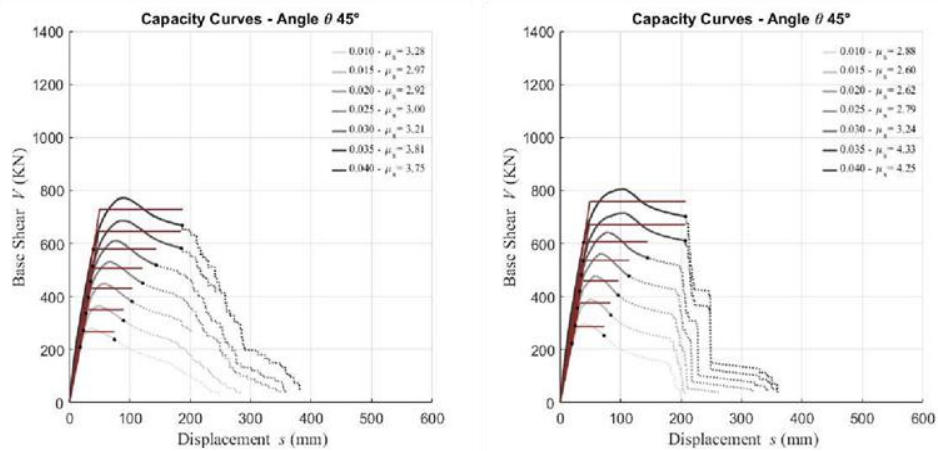


Fig. 10. Comparison between several capacity curves for a model T2 400×400 mm columns section with rebars position according to Fig. 1 (left) and Fig. 9 (right)

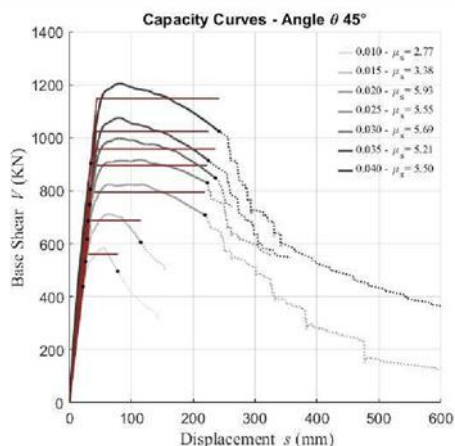


Fig. 11. Capacity curves of model T2 with 500×500 mm cross section columns

Although the design formula has been validated on low-rise buildings, its validity can be extended to three-dimensional beam-column nodes also belonging to medium and high-rise RC buildings. Referring to the second observation, the design rule set out in Eq. (20) will prevent collapses with “H” type mechanism for any direction of the seismic action, with consequent improvement of the ductility values.

8. Conclusions

This work investigates the nonlinear behaviors of two framed RC structures subjected to seismic actions characterized by different propagation directions. The results, obtained through a parametric investigation conducted using OpenSees and Matlab, allow to highlight how the global (displacement) ductility is strongly influenced by the direction of the earthquake, as already observed for the local (curvature) ductility. Structural standards generally require the simultaneous presence of both horizontal components of the seismic action, one at its full value (100%) and the other at a reduced percentage (30%). Nevertheless, this provision does not make available any indication for the evaluation of the critical angle of the seismic action for which the lowest ductility value would be obtained. The results of this investigations also show that as the angle of attack increases, the framed 3D RC structures start to be affected by unwanted collapse mechanisms, such as soft story mechanisms, due to the reduction of the local ductility capacities of the columns. In particular, it was possible to observe that, while for angles of attack of the seismic action of 0° and 15° the prevailing collapse mode is the “L” type, for angles of attack of 30° and 45° the prevailing collapse mode becomes the “H” type. This mechanism, which significantly reduce the excursion in the plastic field, may not be avoided through the application of the simplified procedure provided by current design standards. To overcome this drawback, especially for DCH structures, a further condition to be checked after having defined the longitudinal reinforcements of beams and columns framing into the same joint, has been proposed. It can avoid the formation of a plastic hinge in the columns under the combined effect of the bending moments transmitted to the joints by the beams lying along two perpendicular axes for any direction of the seismic action.

References

- [1] Park R, Paulay T. Ductile reinforced concrete frames - Some comments of the Special provision for seismic design of ACI 318-71 and on Capacity design. Bull N Z Natl Soc Earthq Eng. 1975;8(1):70-91. <https://doi.org/10.5459/bnzsee.8.1.70-90>

- [2] Wilson EL, Suharwardy I, Habibullah A. A clarification of the orthogonal effects in a three-dimensional seismic analysis. *Earthquake Spectra*. 1995;11(4):659-66. <https://doi.org/10.1193/1.1585831>
- [3] Magliulo G, Maddaloni G, Petrone C. Influence of earthquake direction on the seismic response of irregular plan RC frame buildings. *Earthq Eng Eng Vib*. 2014;13(2):243-56. <https://doi.org/10.1007/s11803-014-0227-z>
- [4] Mosleh A, Rodrigues H, Varum H, Costa A, Arêde A. Seismic behavior of RC building structures designed according to current codes. *Structures*. 2016;7:1-13. <https://doi.org/10.1016/j.istruc.2016.04.001>
- [5] CEN. EN 1992-1-1:2004, Eurocode 2: Design of concrete structures - Part 1-1: General rules and rules for buildings. European Committee for Standardization; 2004.
- [6] FEMA. FEMA 356 Prestandard and commentary for the seismic rehabilitation of buildings. Federal Emergency Management Agency; 2000.
- [7] ATC. ATC-40 Seismic Evaluation and Retrofit of Concrete Building. Redwood City, CA: Applied Technology Council; 1996.
- [8] Hosseinpour F, Abdelnaby A. Effect of different aspects of multiple earthquakes on the nonlinear behavior of RC structures. *Soil Dyn Earthq Eng*. 2017;92:706-25. <https://doi.org/10.1016/j.soildyn.2016.11.006>
- [9] Shojaei F, Behnam B. Seismic vulnerability assessment of low-rise irregular reinforced concrete structures using cumulative damage index. *Adv Constr Concr*. 2017;5(4):407-22.
- [10] Ruiz-García J, Yaghmaei-Sabegh S, Bojórquez E. Three-dimensional response of steel moment-resisting buildings under seismic sequences. *Eng Struct*. 2018;175:399-414. <https://doi.org/10.1016/j.engstruct.2018.08.050>
- [11] Dang H, Lee K, Han S, Kim S. Experimental assessment of the effects of biaxial bending moment and axial force on reinforced concrete corner columns. *Struct Concr*. 2018;19(4):1063-78. <https://doi.org/10.1002/suco.201700211>
- [12] Breccolotti M, Materazzi A, Regnicoli Benitez B. Curvature ductility of biaxially loaded reinforced concrete short columns. *Eng Struct*. 2019;200:109669. <https://doi.org/10.1016/j.engstruct.2019.109669>
- [13] Valenzuela-Beltrán RS, Bojórquez E, Chávez R, Bojórquez J, Llanes-Tizoc M. Ground motion selection for the evaluation of residual inter-story drifts in moment-resisting reinforced concrete frame buildings. *Soil Dyn Earthq Eng*. 2020;136:106217. <https://doi.org/10.1016/j.soildyn.2020.106217>
- [14] Zhang C, Tao M-X. Strong-column-weak-beam criterion for reinforced concrete frames subjected to biaxial seismic excitation. *Eng Struct*. 2021;241:112481. <https://doi.org/10.1016/j.engstruct.2021.112481>
- [15] Karki P, Oinam RM, Sahoo DR. Evaluation of seismic strengthening techniques for non-ductile soft-story RC frame. *Adv Constr Concr*. 2020;9(4):423-35.
- [16] Esfandiari J, Zangeneh E, Esfandiari S. Experimental and numerical investigation on RC moment-resisting frames retrofitted with NSD yielding dampers. *Adv Constr Concr*. 2022;13(4):339-47. <https://doi.org/10.1007/s40996-021-00773-x>
- [17] Abdelnaby A, Elnashai A. Numerical modeling and analysis of RC frames subjected to multiple earthquakes. *Earthq Struct*. 2015;9(5):957-81. <https://doi.org/10.12989/eas.2015.9.5.957>
- [18] Wang J, Burton HV, Dai K. Combination rules used to account for orthogonal seismic effects: State-of-the-art review. *J Struct Eng*. 2019;145(11):03119001. [https://doi.org/10.1061/\(ASCE\)ST.1943-541X.0002420](https://doi.org/10.1061/(ASCE)ST.1943-541X.0002420)
- [19] CEN. EN 1998-1-1:2004, Eurocode 8: Design of structures for earthquake resistance - Part 1: General rules, seismic actions and rules for buildings. European Committee for Standardization; 2004.
- [20] ASCE. ASCE/SEI 7-16: Minimum design loads and associated criteria for buildings and other structures. Reston, VA: American Society of Civil Engineers; 2017.

- [21] Dabiri H, Kaviani A, Kheyroddin A. Influence of reinforcement on the performance of non-seismically detailed RC beam-column joints. *J Build Eng.* 2020;31:101333. <https://doi.org/10.1016/j.jobe.2020.101333>
- [22] McKenna F, Scott M, Fenves G. Nonlinear finite-element analysis software architecture using object composition. *J Comput Civ Eng.* 2010;24(1):95-107. [https://doi.org/10.1061/\(ASCE\)CP.1943-5487.0000002](https://doi.org/10.1061/(ASCE)CP.1943-5487.0000002)
- [23] Nguyen QV, Fatahi B, Hokmabadi AS. The effects of foundation size on the seismic performance of buildings considering the soil-foundation-structure interaction. *Struct Eng Mech.* 2016;58(6):1045-75. <https://doi.org/10.12989/sem.2016.58.6.1045>
- [24] Belkacem MA, Bechtoula H, Bourahla N, Belkacem AA. Effect of axial load and transverse reinforcements on the seismic performance of reinforced concrete columns. *Front Struct Civ Eng.* 2019;13(4):831-51. <https://doi.org/10.1007/s11709-018-0513-3>
- [25] Ahmad N, Masoudi M, Salawdeh S. Cyclic response and modelling of special moment resisting beams exhibiting fixed-end rotation. *Bull Earthq Eng.* 2021;19:203-40. <https://doi.org/10.1007/s10518-020-00987-w>
- [26] Ahmad N, Shahzad A, Rizwan M, Khan A, Ali S, Ashraf M, et al. Seismic Performance Assessment of Non-Compliant SMRF-Reinforced Concrete Frame: Shake-Table Test Study. *J Earthq Eng.* 2019;23(3):444-62. <https://doi.org/10.1080/13632469.2017.1326426>
- [27] Chen M, Ho J. Combined strain gradient and concrete strength effects on flexural strength and ductility design of RC columns. *Comput Concr.* 2015;15(4):607-42. <https://doi.org/10.12989/cac.2015.15.4.607>
- [28] Kent D, Park R. Flexural members with confined concrete. *J Struct Div.* 1971;97(7):1969-90. <https://doi.org/10.1061/JSDEAG.0002957>
- [29] Park R, Priestley M, Gill W. Ductility of square-confined concrete columns. *J Struct Div.* 1982;108(4):929-50. <https://doi.org/10.1061/JSDEAG.0005933>
- [30] Chen X, Bai Z, Au F. Effect of confinement on flexural ductility design of concrete beams. *Comput Concr.* 2017;20(2):129-43.
- [31] C.S.LL.PP. Aggiornamento delle norme tecniche per le costruzioni. 2018.
- [32] Papanikolaou V, Sextos A. Design charts for rectangular R/C columns under biaxial bending: A historical review toward a Eurocode-2 compliant update. *Eng Struct.* 2016;115:196-206. <https://doi.org/10.1016/j.engstruct.2016.02.033>